University of Pennsylvania
Center for Sensor Technologies
Philadelphia, PA 19104

SUNFEST REU Program

OPTIMIZED METHODS FOR EARLY CANCER DETECTION VIA OPTICAL IMAGING WITH A REDOX SCANNER

NSF Summer Undergraduate Fellowship in Sensor Technologies
Jennifer Geinzer, Electrical Engineering – University of Pittsburgh
Advisor: Dr. Britton Chance

ABSTRACT

Modern medicine requires more accurate resolution and newer detection methods to properly diagnose cancerous tumors. The purpose of the redox scanner is to utilize near-UV, visible light, and NIRS to image at low temperatures the biophysical signs of cancer, with the ultimate purpose of early detection and diagnosis for human patients. The scanner will perform these functions *in vitro* through 3-D imaging of metabolic redox biochemicals, hemodynamic signals, and injected artificial beacons of a tissue sample at 80 x 80 x 80 μm spatial resolution.

An outdated version of the redox scanner was operational but not ideal; in the scope of SUNFEST, the goal was to fabricate a prototype of an improved device based on the biomedical principles of the old machine, and then validate it in its initial stages by comparison of the actual test samples to the scanner data as modeled in Matlab™.

During the 10-week span of SUNFEST, the project progressed from early development and low functionality to near completion. Several vital system improvements were implemented, to include a new optoelectronics driver circuit to provide reliability, a DOS motor controller to fix critical Windows timing errors, and Matlab™ imaging software. Trial results were promising and signal the possible end of the system design phase. The next phase will involve testing on an animal model to find the efficacy of the sensors on actual biological systems.

Table of Contents

1. INTRODUCTION

In the field of medical imaging, precise diagnosis and treatment of cancerous tumors is a top priority. Modern-day medicine currently utilizes several imaging techniques to detect cancer, including magnetic resonance imaging, ultrasound, and x-rays. These techniques provide excellent anatomical status on the size and location of tumors, but poor functional information on the chemical processes within the target tissue.

Subsequently, many cancers go undetected, and a number of unnecessary biopsies are performed. In the field of breast cancer alone, it is estimated that 10%of patients with cancerous tumors (about 20,000 people) go undiagnosed per year, and approximately 50% of the biopsies done are later found to be benign [1]. These statistics indicate that current diagnostic methods are by themselves adequate for cancer identification. Optical tomography, near-infrared spectroscopy (NIRS) [2], and fluorescence spectroscopy [3] show promising results of illuminating the biochemical processes of tissue, without immobilization of the patient. In future years, these technologies may be coupled with extant techniques to detect, diagnose, and locate cancers with extreme precision. Until then, a medical standard is needed to list the biochemical indicators that definitively designate the presence and status of diseased tissue.

2. GOALS

The goal of the redox scanner is to provide 3-D high-resolution images of the biophysical signs associated with cancer. To accomplish this, visible light, NIR, and near-UV probes are used to examine six reduction/oxygenation (redox) biochemicals, hemodynamic signals, and injected artificial beacons in a given tissue sample. Through the imaging process, the efficacy and sensitivity of monitoring redox processes can be compared to that of metabolic signals and chemical beacons, to create a much-needed "gold standard" of the biochemical indicators for cancer.

This machine is intended for commercial utilization in the health care field. After the initial system design phase, it will be tested for cancer diagnosis in animal models, and eventually will serve as an early detection and biopsy tool for human patients.

3. BACKGROUND

The six metabolic, hemodynamic, and molecular target beacons observed by the redox scanner are chosen exclusively for their individual imaging characteristics, as well as their ability to cross-reference one another. The chemicals intrinsic to the human body include mitochondrial nicotinamide adenine diphosphate (NADH), mitochondrial flavoprotein (Fp), oxygenated hemoglobin (labeled Hb_O for this experiment), and total hemoglobin (Hb_T); the two extrinsic signals are the biochemical indicator dyes Cy5.5 and Indocyanine Green (ICG). These signals are imaged in one procedure at explicit temperatures that provide optimal emission and scanning conditions to ensure accuracy of cancer detection.

3.1 Chemicals Observed

Of the four intrinsic properties under study, the two redox chemicals are reduced NADH and Fp. Cells employ these chemicals in metabolic processes. In the biomedical field, it is common knowledge that cancer-induced hyper metabolism causes tissue hypoxia. This in turn decreases the amount of Fp (oxidized) and increases the presence of NADH (reduced) in tumor tissue.

Fluorescence emission spectroscopy can be employed to observe these properties,. In 1958, Chance and Baltscheffsky reported that NADH from the mitochondrial matrix auto fluoresces to a wavelength of 450 nm when tissue is excited with light of wavelength 366 nm [4]. Similarly, mitochondrial Fp emits light in the oxidized form at 520 nm with an excitation of 460 nm. In conventional methods of analysis, a redox ratio of NADH/Fp is calculated and then compared to a standard. Figure 1 illustrates the key locations of excitation, reflectance, and fluorescence emission spectra in the visible spectrum for the six chemicals under investigation.

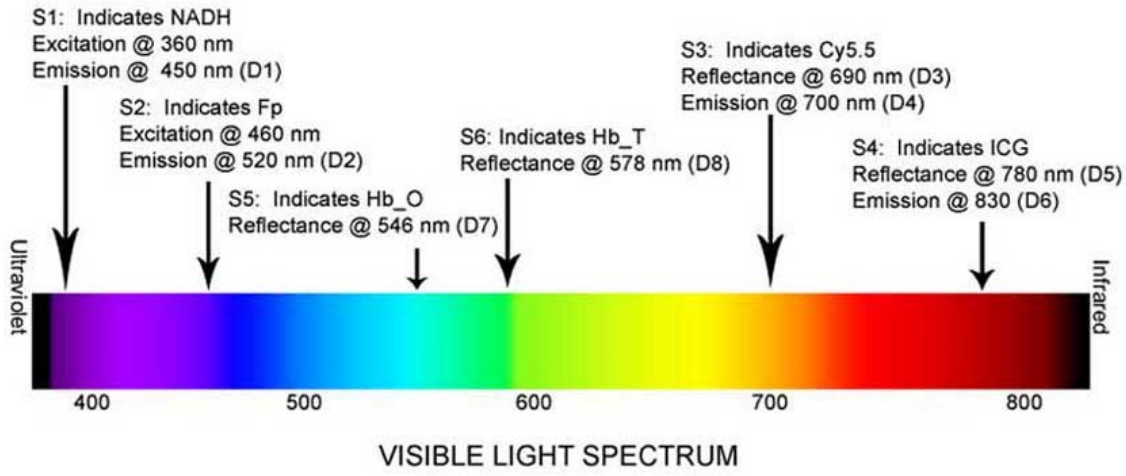

Figure 1. Source 1 (labeled S1) and S2 emit wavelengths in the near-UV and indicate redox chemicals, S5 and S6 create light in the visible spectrum and indicate molecular target beacons, and S3 and S4 provide NIR light and show hemoglobin.

Tissue health may also be evaluated by observing hemodynamics. Hb_O reflects light at 546 nm, and Hb_T reflects 578 nm light. Research in progress has indicated that malignant tumors show a low ratio of Hb_O/Hb_T when compared to healthy tissue, but benign tumors may show a normal to high ratio of the two [1]. Therefore, hemodynamics could be useful not only in detecting cancer but also in determining the difference between metastatic, malignant, and benign tumor types.

The two extrinsic probes used in this experiment are indicator dyes introduced to the tissue via localized or venous injection. ICG is a blood vessel indicator, and Cy5.5 is a cathepsin B indicator. Angiogenesis, the creation of new blood vessels, increases the bloodflow in a particular region, and thus increases total hemoglobin. The ICG beacon

can be cross-referenced with the previous two signals to understand hemodynamics more fully. The presence of the enzyme Cathepsin B has been shown to signify the presence of HT1080 type mouse cancers in recent experimentation [5]. The two indicator dyes both fluoresce and reflect light; Cy5.5 reflects light at 690 nm and fluoresces at 700 nm, while ICG reflects at 780 nm and fluoresces at 830 nm. Imaging of these beacons will indicate quantitatively how effective they are in molecular bonding and pinpointing tumors.

3.2 Temperature Specifications and Effects on the Scanner

Cryo-imaging has multiple advantages over scanning at room temperature. For this reason, the redox scanning procedure calls for the imaged tissue samples to be freeze-trapped and cooled with liquid nitrogen to 77 K. Molecular signals move very quickly toward the reduced state if the host tissue reaches temperatures over –20°C [6, p.15]. Freeze-trapping prohibits new oxygenation and metabolism of the test sample, enabling researchers to look at one biochemical "snapshot" in time. At liquid nitrogen temperatures, tissue is hard enough to be mounted and mechanically ground with standard steel milling tools. In addition, low temperatures have been proven to enhance tissue fluorescence [7], allowing greater signal transmission and thus provide greater signal-to-noise ratio for the fluorescing chemicals.

The extremely low temperatures significantly affect the operation of the opto-electronic components of the system and must be taken into consideration. Simple imaging methods where the source and detector pairs are very close to the scanned medium are impractical at these temperatures because of their severity and the sharp 221 K temperature differential between the immediate vicinity of the sample and the ambient temperature. If the sources and detectors are moved away to shield them from the temperatures, they will not provide the necessary 80 μm resolution due to diffusion of the light.

The solution to this problem is to use a light guide. The redox scanner utilizes one constructed from 14 fiber optic cables—six source fibers of 1000 μm each were connected around the circumference of a coupling, and eight detector fibers of 100 μm each are located in the middle of the coupling. The optimal design of the fiber tip coupling is shown in Figure 2.

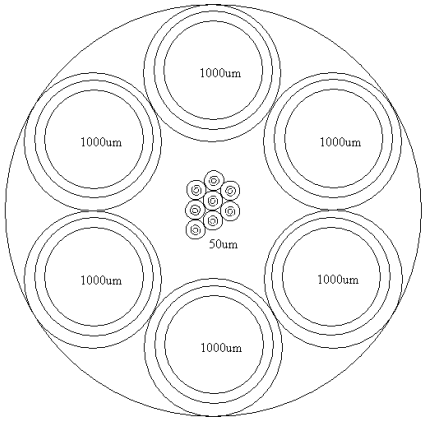

Figure 2. To maximize transmission of light through the fiber optics, the coupling is designed so the six source fibers surround the eight fibers.

The final component affected by the temperature conditions is the grinder. Before the cutting blades come in contact with the sample, both must be the same temperature. This condition is attained by immersing the blades in liquid nitrogen prior to the initial grind sequence.

4. SCANNING PROCEDURE

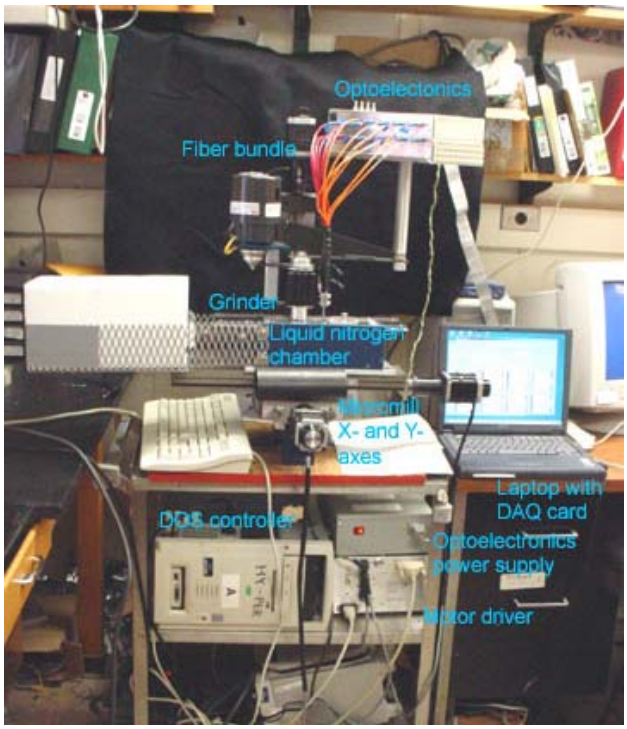

Figure 3. The main components of the redox scanner, to include the movement system, optoelectronics, and laptop, are labeled above.

In future testing, a tumor will be fostered on an animal model, and will subsequently be freeze- trapped, removed, and then mechanically secured with a chuck in a custom-built liquid nitrogen chamber. Figure 3 labels each component of the system. The liquid nitrogen will then be poured into the bottom of this chamber, freezing the chuck into place and keeping the tissue sample at low temperatures. The tumor is then prepared for scanning.

The imaging procedure is accomplished through use of the three main components of the redox scanner: the movement system, comprised of the MicroMill 2000™, driver, and a DOS controller; the opto-electronics; and a NI-DAQ™ PCMCIA-1200 card interfaced to laptop. The DOS controller is a recent addition to the system, and will be discussed in greater detail in Section5.5.

4.1 Mill and Motion

The MicroMill 2000™ is a standard hobbyists' milling tool that provides all of the movement required for the scanner. The mill shifts the liquid nitrogen chamber fitted to the x- and y-axes, and controls the vertical movement of the fiber optics and a 12-blade grinder on the z-axis.

The specific types of motors used for this platform include three 4-phase unipolar stepper motors enabled with half step mode. Each motor controlling one axis is run by four solenoids in the up, down, right, and left positions. Whenever the software provides current through any one or two coils simultaneously, the resulting magnetic response turns the gears. This allows eight steps of motion—the four cardinal phases, and the half steps in between. While the programming code provides a series of pulses through the driver to successive clockwise or counter-clockwise (cw/ccw) coils, the motor moves the nitrogen box in a positive or negative direction. As with any gear-based transport system, the mill cannot be run from a halt to a fast speed, so the velocity must be ramped with a constant acceleration. The motors can move the axes and grind with a step increment as

small as 3.175 μm. The axes also have knobs for manual control, while the motors are unpowered.

Affixed to the x- and y-axes are a Styrofoam™ filling chamber for adding liquid nitrogen as well as the Plexiglas® nitrogen chamber that houses the tissue sample. A chuck is fitted on the inside of this box to secure the sample. The optics bundle is held securely by the z-axis. The entire scanning sequence is run by the laptop via the "RedoxScanner" Microsoft Visual C++™ (hereafter referred to as VC++) software developed by the lab and a DOS computer.

The sequence begins by immersing the grinder in liquid nitrogen. The laptop prompts the user to run an initial calibration algorithm, and then the mill calls for the initial grind: It moves the sample underneath the grinder, smoothing out the top layer of the tissue.

The actual scanning motion begins after the sample is repositioned so that the optics bundle hovers over the top left corner of the sample. The sample is scanned from top to bottom (horizontally), and then the sample is moved left, reset to the top, and so on for a total of 128x128 pixels/cm^2 sample surface. The user can alter this scan size as needed.

Since the mill uses stepper motors, there is some play in the gears when shifting directions along one axis. To ensure that the starting position of each scan is on the same coordinates, after scanning down (horizontally) 128 pixels, the reset subroutine calls for fast movement of 133 pixels up and five back down to the y-axis start position.

After the first slice is scanned, the grinder removes 80 μm of tissue, and the scanning process restarts. The end result is eight tissue slices per compound, for a total of 64 images. These can then be analyzed to get a 3-D view of the biochemical, physiological, and metabolic processes of the tissue.

4.2 Optics and Data Acquisition

The optoelectronics and data acquisition funcion as follows. A National Instruments™ PCI 1200 data acquisition (DAQ) card is connected to a Windows 2000™ laptop. The "RedoxScanner" software supplies the light sequence in the form of voltage pulses, which are shuttled through the DAQ card to the driver circuit. The signals then run the light sources in the manner determined by the timing diagram. The flowchart and timing diagrams illustrate the steps in the process, see Figure 4 on the following page. The timing sequence for the sources labeled S1-S6 is {S1, S2, S3, S3, S4, S4, S5, S6}. Source 3 and S4 are given two pulses each, as they excite tissue such that it has both a reflection and fluorescence response. These two responses are measured by separate detectors. To generate near-UV light, SpectraLEDs are used for S1 and S2. The NIR S3 and S4 signals are provided by laser diodes, and S5 and S6 in the visible spectrum are provided by green and yellow LEDs.

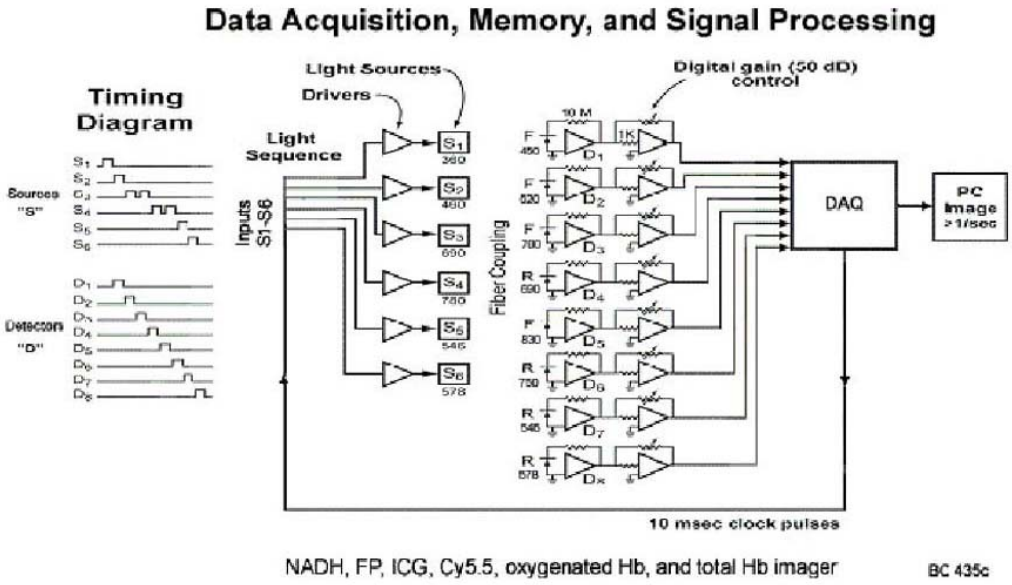

Figure 4. Light pulse timing is supplied by the DAQ card, as shown in the flowchart and the timing diagrams. Since the artificial molecular beacons Cy5.5 and ICG (light provided by S3 and S4) both reflect and fluoresce, they have two detectors each to measure these responses.

The light sources are held perpendicular to and flush against optical fibers. This light guide is secured by the mill, and is held 80 μm above the surface of the sample to maximize photon transmission and for the appropriate resolution. The light is then either reflected or fluoresced and transmitted back through the detector optics. Fluorescence signals are detected by photomultiplier tubes (PMTs), and the reflected light is measured with OPT101 photodiodes.

The DAQ card runs the sampling of the detector sequence simultaneously with the source sequence, in the manner {D1, D2, D3, D4, D5, D6, D7, D8}. These signals are amplified and then sent to the DAQ, where the data are converted from analog to digital, processed through an averaging filter, and output as a *.txt file. The resultant data can then be imaged by Matlab™. The current data acquisition calls for eight averaged samples taken per pixel, for a total of 16384 pixels and a spatial resolution of 80 μm. The entire scan sequence takes approximately 6.7 hours, which is 50 minutes per slice, or 183 ms per pixel.

5. TESTING AND EVALUTATION

This project is a work in progress, so all work accomplished, intermediate results, and debugging are presented here.

By the beginning of SUNFEST 2003, the macroscopic designs and specifications had already been determined. As an updated prototype of an older redox scanner, the

128x128 pixels/cm^2 (80 μm) resolution had been concluded to be optimal. The primary researchers in the lab had decided to add ICG, Cy5.5, Hb_O, and Hb_T to the list of scanned chemicals. The mill was already assembled, the liquid nitrogen box was built, VC++ code to run both the mill and the optics had been written, the fiber optics bundle had been coupled, and a first driver circuit had been constructed.

The following sections discuss the solutions and troubleshooting for various software and hardware problems observed in the system.

5.1 Software Calibration Bugs

During the first tests of the graphical user interface (GUI) for the mill, the original motion and calibration sections of the VC++ code prevented the end user from completing the calibration sequence. This problem stemmed from confusing conventions used to designate the axis motion, and the incorrect documentation of this movement. The "MMTest" code, designed to test the axes and familiarize the user with the positive and negative conventions, contradicted the "RedoxScanner" code concerning directional mapping.

The mechanical movement system on the mill was difficult to visualize, which exacerbated the situation. To scan, the fiber optics system that sampled the data was stationary while the box and the grinder moved, which was a somewhat unorthodox configuration. In addition, the knobs on all the axes did not turn clockwise or counter-clockwise consistently to move in any "positive" labeled direction.

After several false starts, it was determined that the easiest way to picture the system was to relate the horizontal x- and y-coordinates to standard graphing axes. It was important to note that the x and y direction conventions were taken with respect to the movement of the liquid nitrogen box underneath the optics. Facing the mill, the "positive" motion was right for the x-axis and up for y-axis. On the z-axis, vertical up and down moved the grinder and the optics in those directions. These conventions are illustrated by Figure 5 .

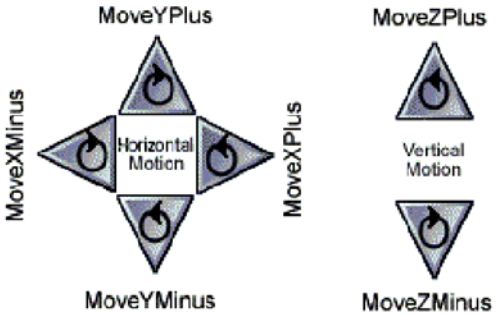

Figure 5. Directions are shown by the arrows and their corresponding VC++ functions. The circular arrows indicate the cw/ccw turning of the axis knob when moving in that direction.

Viewing the system from the perspective of the optics and sample provided an entirely opposite and wrong orientation. For instance, if the box moved left on the axes, the fiber tip over the sample moved right.

Several coding errors were discovered in the original programming based on direction assignments. In the initial calibration instructions, the final segment of code would not allow the user to move the box in the left direction and thus set the sample in the correct initial scanning position. This error was rectified, and the user was given more precise control during calibration. By altering the GUI, the motion code, and demonstration graphics for clarity purposes, the process was simplified. A glitch exhibited through faulty z-axis control on the grinder was located and corrected. In the original code, the x-axis movement was insufficient to smooth the entire sample. This could have lead to errors in the scan data, so the distance of the grinding sequence was lengthened.

5.2 New PCB Source and Detector Driver

The first circuit built to control the light sources and detectors never operated satisfactorily. The design for this printed circuit board (PCB) was pieced together from previous circuits in the lab that were built for the purpose of imaging, but incorporated a feature that was unnecessary for the purpose of the redox scanner—a sample and hold architecture inherited from a Time Resolved Spectroscopy system. The biological tissues that will eventually be imaged by the redox scanner system will be static, both physically because they will be *in vitro* and chemically as a result of the flash freeze process, so there is no time-dependency. This extraneous portion of the old circuit reputedly caused the most problems in the system.

A new version of the circuit was designed with Protel™software and sent to Advanced Circuits to be manufactured. Several items were updated in this version, including the deletion of the sample and hold construction. The circuit layout was also improved to provide for easier troubleshooting. Figures 6 and 7 illuminate the layout and final design of the circuit. After the new PCB was received, some additional work was required to make the circuit operational. The various components of the circuit were soldered to the board, and individual LED driver circuits were constructed and connected to the system. The old sample and hold architecture called for different source and detector timing, so the "RedoxScanner" software was updated to reflect the new sequences (shown in Section 4.2).

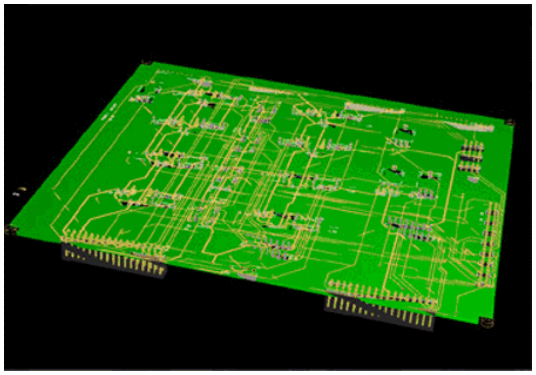

Figure 6. A model of the PCB was constructed via CAD software. The figure reveals how the circuit looked prior to adding electrical components.

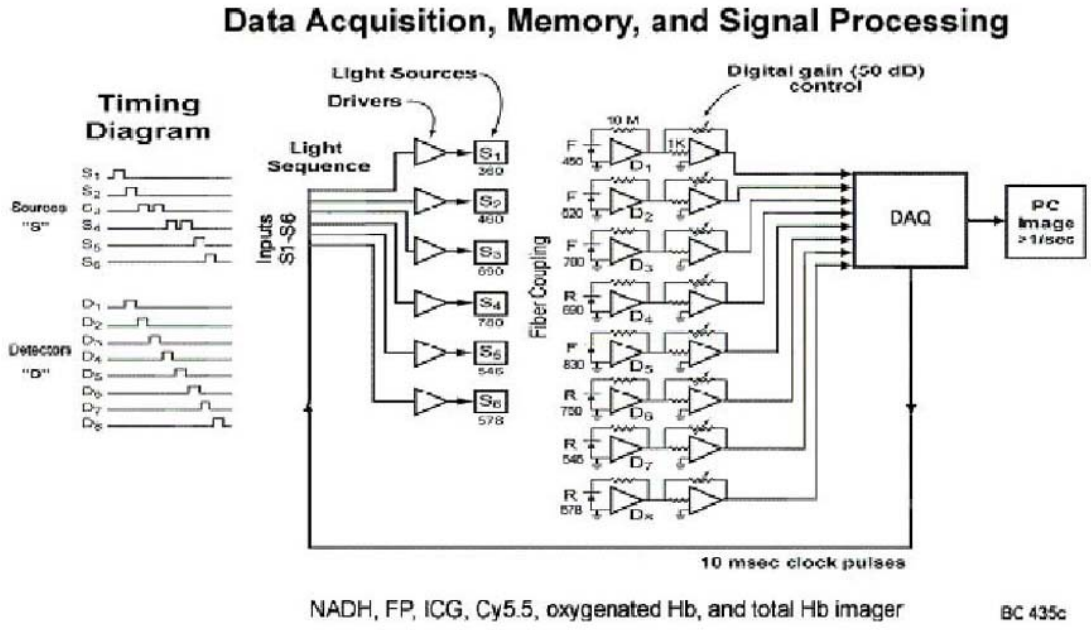

Figure 6. The new PCB schematic was designed with Protel™ prior to its manufacture. In the upper right are the DAQ card connections, below that are the high voltage power supplies for the PMTs, to the center are the source and detector busses; on the bottom center are various other power supplies, and the left shows the amplifiers for the signal outputs.

5.3 High-Signal Attenuation and Noise

5.3.1 Initial trial of redox scanner

After the new PCB was implemented and tested, the redox scanner was equipped to record its first image. To prepare for the trial run, the PMTs and photodiodes were exposed to a controlled amount of white overhead fluorescent lighting, and the voltage output was evaluated with a multimeter. This verified that white light, stronger than any signal that would be provided to the system, output nearly 5V, which is the maximum allowed by the system. Source 1 of wavelength of 360 nm fluoresced on bright white paper, and at 460 nm, S2 fluoresced with yellow highlighter. At the time, S1 and S2 were the only operational sources, so they were tested with a very simple standard—a smiley face drawn on bright white paper with black marker. This standard was affixed to the top of a plastic block held in place by the chuck. The hypothesis was that the output from D1 would be clearer than that from D2, since white is the optimum color for fluorescence of S1 and not S2. Results were achieved by using the default setting of 128x128 pixels/cm^2, with the number of slices set to 1 and the distance from fiber tip to sample under 1 mm (a method to calibrate this height to 80 μm has not yet been determined). The fiber tip was lowered closer to the sample in Trial 1. The testing outcomes are demonstrated in Figure 8.

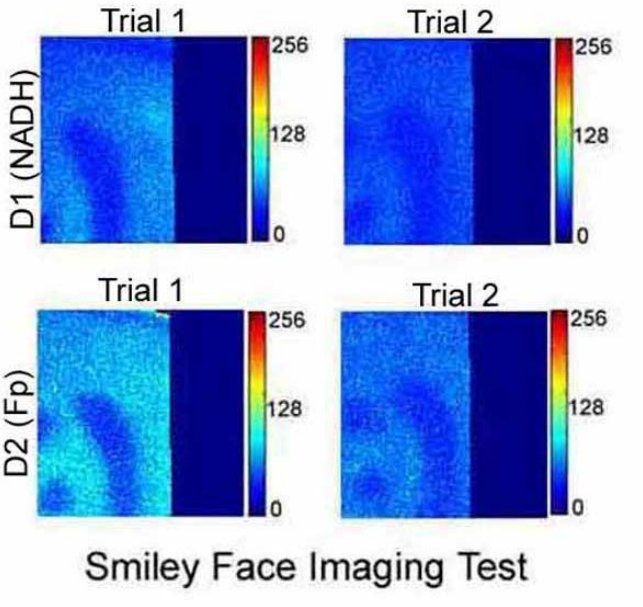

Figure 8. Red corresponds to the maximum output signal from the imager, and dark blue designates zero signal. Based on this scale, these two tests indicated very low signal-to-noise ratio. The rectangular areas signifying no signal on the right of the samples corresponded to times when the scan cycle was intentionally interrupted.

Comparing the images from the two different sources elucidated the capabilities of the circuit up to that point. The images clearly indicated that S2 experienced better signal transmission than S1, which contradicted the hypothesis, but was a reasonable result. This signified that not all source and detector fibers in the optics could be used interchangeably. If the distance between the fibers was too large, little or none of the signal was transmitted

These observations have established the methods for further testing. In future trials, pairs with more similar/better output characteristics should be chosen. The intensity of the images from two different light sources may not be directly comparable without a significant amount of calibration. The initial step in the trial should have been to calculate the offset (the noise measured when the detectors are held in complete darkness) via the VC++ software. This was not accomplished in these tests due to the difficulty of transporting the prototype to a dark room.

Performing this test in the future should eliminate small inconsistencies between the detectors, but still will not ensure that each signal will be amplified equally. To accomplish this, the scanner should be calibrated prior to use with a standard having a known value for each of the six chemicals. By scanning the standard prior to actual use, the intensity of the signals could be adjusted in the software to show an empirical, rather than a relative, voltage output.

The images indicated that other seemingly trivial distances also played significant roles. As the distance from source to sample decreased (starting from under 1mm), the signal transmission increased as long as the source-detector distance in the fiber was small. The intensity of the signals from the first trial was noticeably higher, thus reconfirming that 80 μm was a reasonable depth for good transmission. In addition, the separation between individual detectors meant that while the scanned areas overlap, the images from two chemicals would not show the same 128x128 pixels. Compared to the D1 image, the D2 image was shifted a great deal to the left. This finding lent further weight to the argument that output signals from different chemicals were not immediately comparable.

The core issue was that the signal-to-noise ratio was far too low. Ideally the lights should fluoresce very strongly with a white standard. Even the strongest signal from Fp did not show half of the maximum output voltage, which was unacceptable for accurate imaging.

5.3.2 Light guide signal transmission

Many factors contributed to the low signals. One issue involved the transmission of the light through the source optics, and the subsequent reflectance of the signal back into the detector fibers. The fiber tip coupling was designed to have the symmetry shown in Section 3.2 Figure 2. Note that in this design, there was one source fiber close in distance to at least one detector fiber. All source/detector pairs would have a similar separation distance.

Because of the difficulties of manufacturing such an optics cable, the machine shop was not able to build the coupling to the specifications. In the real fiber coupling, all the detectors were bundled together in the middle and toward one side, so that they nearly touched two of the source fibers. This greatly affected the transmission of the signals, as shown by the following evaluation of the optics.

To test which source and detector fibers should be combined to maximize output signals, a green LED (578 nm) signal and a specific photodiode were employed to evaluate each individual combination. The six source and eight detector fibers were labeled alphabetically for ease of identification, and a mirror was used to simulate absolute reflectance conditions of the sample. The tests were conducted with a fiber tip/sample separation of under 1 mm. With the "RedoxScanner" software running, the DAQ card supplied a pulse train throughout the system. The voltage output from the photodiode detector was measured with an oscilloscope set for data averaging of 16 samples. The results are shown in Figure 9 below.

		Source Fibers (Red)					
Detector Fibers (Orange)		**A**	**B**	**C**	**D**	**E**	**F**
	A	2.16	1.44	0.00	1.28	0.00	2.80
	B	0.00	0.00	0.00	6.80	0.00	5.84
	C	0.00	0.00	0.00	1.76	1.20	3.52
	D	2.80	1.72	0.00	1.68	0.00	6.80
	E	2.96	5.52	0.00	0.00	0.00	1.52
in mVpp	**F**	5.96	2.16	0.00	0.00	0.00	3.04
	G	0.00	2.24	1.20	0.00	1.20	1.44
	H	0.00	0.00	0.00	1.68	0.00	8.80

Figure 9. The highlighted output signals were the only ones completely distinguishable from the system noise. Source fibers F and A transmitted light such that multiple detectors could identify the signals, but Sources C and E did not have any detectors capable of sensing any signal. This signified that the fiber coupling geometry was not usable for the purposes of the redox scanner, since all fibers were necessary for experimentation.

It was important to note while the signals were very small, this was directly related to fiber tip/sample separation. An output voltage difference of up to two orders of magnitude larger was detected by adjusting this separation, so the results of this test are relative, not empirical. The relationships between the source and detector transmission remained constant at all separations however, so this test was a valid indication of coupling quality.

The yellow highlighted values specified the voltage pulses that were definitively distinguishable from the system noise. Two of the source fibers, C and D, do not have any detectors that transmitted the signal. This was a major problem, and indicated that with the current fibers two of the signals cannot be transmitted. On the other hand, fibers A and F conveyed signals well through multiple fibers. Making an informed estimate of the geometry of the system, it was concluded that source fibers A and F were the closest to the detector bundle, source fibers B and D were touching A and F to either side, and source fibers C and E were the farthest from the detectors.

Recoupling the fibers would be an expensive and time-consuming process, so the faulty optics configuration was used for the remainder of the SUNFEST program. The source and detector pairs were chosen through results from the chart to enhance transmission as best as possible with the extant geometry.

In addition to the combined source/fiber coupling problem, the coupling on the other end between individual fibers and the detectors was flawed. For the optimal configuration for signal transmission, the fibers were screwed into a coupling in the optoelectronics box. The fiber tips would then be secured flush against and perpendicular to the detectors. In practice, an acceptable signal could be transmitted only when the fibers were adjusted in the couplings by hand during the scanning process. Inspection of the couplings revealed that they were too long, causing a gap between the fibers and detectors. Cutting down the threads on the coupling removed this distance and greatly enhanced the signal.

5.3.3 OPT101 photodiode and LED efficiency

The efficiency of the OPT101 detectors was evaluated with the goal of enhancing the signal through other means. In the smiley face test, it was noted that the output signals from the green LED (578 nm) were extremely small. The output voltage of a yellow LED (546 nm) was assessed to find the signal was only slightly larger than that from the green LED.

The OPT101 specifications were reread to reveal that they were not optimal for detecting signals from the green and yellow LEDs. An ideal 850 nm infrared light source was expected to have an output of 0.60V/μW. The output decreased linearly with decreasing wavelength, such that the yellow LEDs could be expected to have a signal of 0.375 V/μW and the green LEDs 0.30V/μW, half of the optimal output voltage. After briefly evaluating the option of choosing different detectors that focused on the yellow and green wavelengths, the idea was discarded. The new PCB design was created

specifically to use the OPT101s, and the alternate pinout arrangements and voltage requirements of different detectors would have made it very complicated to integrate them into the chip.

It was ascertained that the best way to increase the output signal was to maximize the power output of the LEDs. Since the signals would be pulsed and not continuously powered, a new driver circuit using a BJT and various resistors was designed to run the LEDs at the high end of their power specifications. This circuit increased the LED supply current to 45mV (where $I_{peak\_max} = 50mV$) and the voltage to 3.0 (where $V_{green\_max} = 4.0$, $V_{yellow\_max} = 3.0$).

Several other measures were taken to increase the signal-to-noise ratio. To augment the voltage signal after the detectors, the feedback resistor on the amplifier was replaced with one of much higher value, 22MΩ. This linearly increased the amplification, but only increased noise by the square root of 22M, giving a signal-to-noise ratio of 5:1. During the testing process the photodiode output signals were discovered to have a high-frequency noise. To eliminate this, RC low-pass filters using 2.2μF capacitors and 1.1MΩ resistors were added to the circuit after the output voltage amplification.

The end result of all the troubleshooting was that the output signal was much improved, but still did not have the clarity and magnitude desired for accurate scanning.

5.4 Matlab Image Processing

The only imaging software that existed for the scanner was the status monitor on the "RedoxScanner" GUI. The "Redox" imaging program was constructed with Matlab v.6.1™ to reliably image and save in picture form the output from VC++. A screenshot detailing the "Redox" GUI appears in Figure 10.

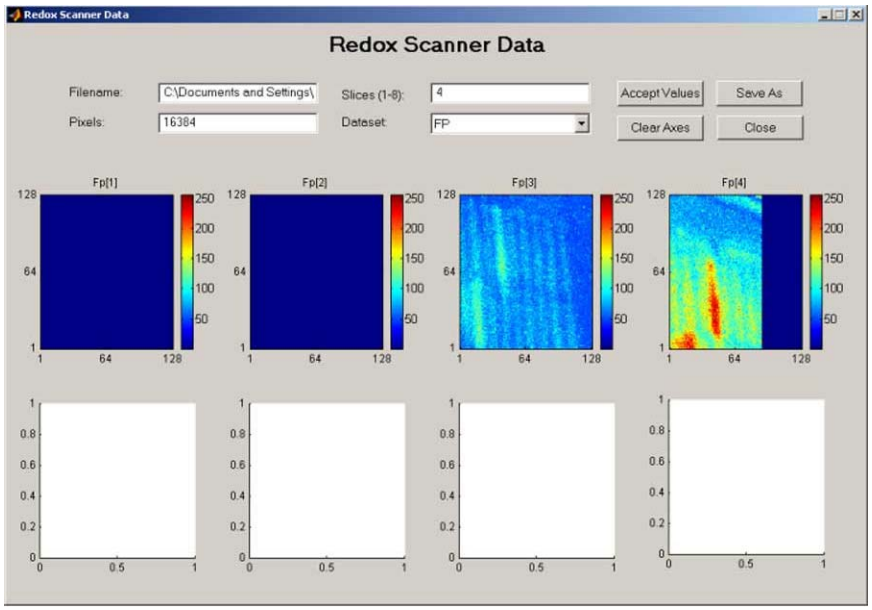

Figure 10. The Matlab™ "Redox" imaging software was designed to be as user-friendly as possible, and to show as many or as few slices of a sample that a user specifies. In addition, it was intended to resemble the VC++ GUI for simplicity.

The layout of the Matlab™ GUI was designed to look similar to the VC++ GUI; however, there were several notable differences. As with the VC++ software, the end user was presented with pictures of up to eight slices at one time, but all these slices were of the same chemical, rather than being specific slices of all chemicals. Since the amount of chemical present in tissue changes with depth, this layout was determined to give clearer information about tissue health. Through the GUI the user could open the *.dat output file for any scan sequence and set the number of sample pixels, the number of slices, and the chemical under observation.

The data were then imaged in the following manner. The number of pixels entered by the user was interpreted as a square sample size. The *.dat file information consisted of voltage values between –1000 and 4096, which corresponded to a signal output of –1 to +5V multiplied by 1000 by the DAQ card and coded in binary. Each pixel voltage value was imported into a matrix and rescaled to have a color value between 0 and 256. These data were printed out to the screen with a colorbar to show the color to intensity scale.

The user could then choose to view another chemical from the same scanning sequence, or select data from another scan sequence and reset the number of pixels and slices accordingly. The images are saved separately to a *.tiff file in a user-specified path.

5.5 Windows Timing Delay Causes Motion Lag

The original hardware configuration was a compromise between two system configurations. The Micromill 2000 was designed only to run under non-Windows DOS. The DAQ card was supported only under Windows™ platforms. Non-Windows DOS cannot run programs simultaneously with Windows on one computer, so the VC++ code had been created to bridge the two and run the mill under Windows-based DOS. Thus in this hardware arrangement, a Windows 2000™ laptop ran the optoelectronics through the DAQ card and simultaneously supplied pulses to the Micromill driver through the serial port. This configuration caused the most critical problem in the system, and was the most difficult to debug.

5.5.1 Initial hardware and software debugging

During the initial calibration of the Micromill prior to scanning, the motion along the x-axis was inconsistently choppy. In the original configuration, all the Micromill motion was controlled directly by the “RedoxScanner” software. Believing the lag to be a software issue, the calibration code was examined. The function FastMoveX() was responsible for the specific movement in question, but the other places where it was used did not seem to replicate the choppy motion. The DAQ card specifications verified that it was being utilized to the bottommost level of its capabilities, eliminating the possibility of a buffer bottleneck.

The next course of action was to investigate a hardware issue. When the machine was first implemented, the mill experienced similar lagging problems. These were

resolved by running the mill at a steady rate for approximately 36 hours to prime the machine. The mill had not been operated for several months prior to the new problem cropping up, so repriming the machine seemed a feasible solution. The machine was lubricated and simple VC++ test code, "MMBurnIn," was then written to ramp the mill to a high speed and then decelerate back and forth across the x-axis 500 times. Observation of the final sequences verified that the x-axis movement had not improved.

The proprietary "MPS2000" DOS Micromill software was then evaluated to determine whether the problem stemmed from the VC++ or a hardware malfunction. Simple G-code programs were coded to provide x-axis movement in the DOS software. At that time DOS could be run only from a Windows shell. When asked to move slowly the program behaved correctly, but when supplied a very fast ramp the motion was again choppy and the gears ground. To confirm that the problem was necessarily with the x-direction, the signal outputs to the x- and y-axis motors were switched from the power supply, and consequently the y-axis behaved erratically. This indicated that the problem was not in the VC++ code or in the Micromill 2000 hardware.

A series of tests was then conducted on the control signals from various hardware sources. The Micromill driver box that drove the motors was dismantled and probed with a multimeter, which did not provide any useful information. The graycode outputs from the DAQ card were tested with an oscilloscope. The DAQ was assessed using the "MMTest" software, causing the graycode to step by mouse click event, and the signals were found to be very clean 5V ramp functions. In hindsight, the frequency of the "RedoxScanner" graycode should then have been evaluated, which would have immediately explained the problem. Instead, this line of evaluation was suspended.

5.5.2 Grid imaging test

An experiment was conceived to find both the accuracy of the x- and y-movement and the affects of the lag on the sampling. The analysis methods used to capture the previously mentioned smiley faces were replicated here, with the exception of a different standard. Again, S1 and S2 were the test sources. A 1 cm^2 grid was drawn on bright white paper with a black fine-tipped pen. The grid consisted of vertical lines drawn every 2 mm, and horizontal lines drawn at the top, 5 mm down, and at the bottom of the grid. Two of the resulting rectangles were colored in with fluorescent yellow highlighter to test S2 fluorescence. The results of three different scans are shown in Figure 11.

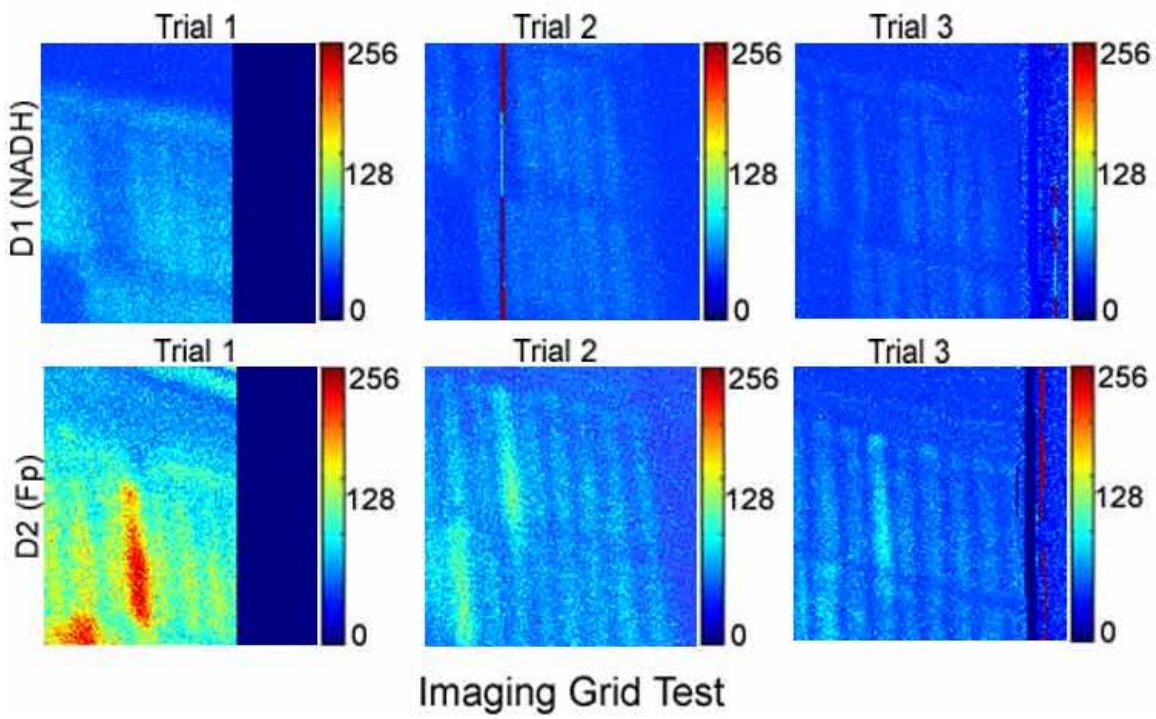

Figure 11. When imaged in the "Redox" software, the data denoted that the scanner had interpreted the grid as slanted lines. This proved that data had been lost somewhere in the scanning process, and and gave credibility to the theory that the delay was a Microsoft Windows problem.

These test results echoed those of the previous test in several ways. Source 2 revealed much better signal transmission than S1, as replicated in the smiley face test, and the dependency of signal to fiber height was firmly established. But the smiley face test utterly failed to convey one major fact.

In Figure 11 the images show straight vertical lines, signifying that the standard was placed straight on the sample bed. However, all the pictures reveal the center line to be slanted diagonally up and to the right, rather than at 90° to all the intersecting vertical lines as it was drawn. This demonstrates that not only are data lost in the process, but that it must occur during the y-axis movement as well, because no data are acquired during x-axis movement.

From all the evidence, troubleshooting, and process of elimination, it was ascertained that Windows™ timing itself caused the lag. The clock pulses provided by the OS did not have consistent timing frequency (which we could discovered earlier by testing the graycode). A consistent frequency is required only for acceleration and deceleration, which explains why the fast movement was affected while normal motion was not. It was now apparent that the Micromill could not be run directly from the laptop, so the system necessitated re-engineering.

5.5.3 Implementation of DOS controller

As recommended by the Micromill manufacturer, an alternative design was established that employed a DOS computer to function as a controller for the motors, isolating Windows™ from Micromill timing. DOS, unlike Windows™, does not multi-task, and thus could time pulses very accurately. The laptop was connected to the DOS box via serial cable, and the DOS computer was linked to the Micromill motor driver through its parallel port.

The VC++ software was updated, and new software was developed to interface the laptop/DOS and DOS/driver systems. In the new VC++ serial port protocol, the laptop passed five bytes to the DOS box every time a new movement was requested. The first byte could be one of two binary numbers. A value of 64 designated the most significant bit (MSB) of a new codeword, and 128 specified a reset. When the "RedoxScanner" program was closed, it output a 0 byte to the system. The DOS box read the 0 and output a 128 to clear previous values. The second byte signified the direction of the movement. The directions {X+, X–; Y+, Y–; Z+, Z–} were coded by {1, 8; 2, 16; 4, 32}. The third, fourth, and fifth byte determined the distance traveled in the direction requested. For each byte, the first six least significant bits were employed for distance, for a maximum of 262,143 steps per codeword. The two MSBs were purposely left blank, so they could not be misconstrued as 64 or 128. The DOS box sent a signal confirmation back to the laptop while the codeword was processing. It then provided the Micromill motor driver with all the timing and signal pulses required for motion along the axes.

This system was newly implemented, but initial testing confirmed that it completely solved the fast motion lag. The laptop could now devote more processing power to data acquisition and seemed to read the grid standard accurately, although no data are currently available to demonstrate this.

6. RECOMMENDATIONS

There are still several major topics to be addressed. The picture quality must be increased, and the optics coupling must be redesigned. Recoupling may increase the output voltage significantly and solve the signal attenuation problem, thus increasing image clarity. During testing, an interrelationship was noted between the source-to-detector distance, the fiber to sample distance, and there may have been a dependence on wavelength as well. This should be calculated ideally as well as empirically to determine the exact geometry of a new fiber coupling to optimize light transmission.

Better image quality can be attained through additional means. To increase the signal clarity, the VC++ software can be set to average more samples per pixel. The DAQ card uses only a small percentage of its processing capability, so the averaging could be increased from 8 samples per pixel to 50 or 500 if there is no resulting lag on the laptop. Also, using smaller-diameter detector fibers in the redesigned fiber coupling will provide increased resolution when the software is adjusted for a smaller step size. However, a

smaller fiber will be even less likely to transmit light, so the transmission characteristics should be calculated carefully to decide if this is feasible before implementation.

Several minor glitches in the VC++ software must be fixed. Currently, the software divides the number of slices by the assumed sample depth (1 cm) to calculate the depth of the sample grind. For instance, in a scan with eight slices, the depth of each grind will be 1/8 cm. The grind depth should be set at a constant value of 80 μm. Also, when the user enters a scan size other than 16384 pixels, the computer does not interpret this as a square image. Instead, it scans down 128 pixels for as many rows or partial rows as needed for the new scan size. This is not necessarily a problem, but is inconsistent with the Matlab™ imaging software, and one should be altered to match the other. In addition, the code was designed with the idea that the voltage output would vary from 0 to +5 V. The DAQ card ideally is set to unipolar, which scales these data in binary to a value between 0 and 4096. In practice the outputs from the DAQ are only multiplied by 1000, and can range from –1000 to approximately 4200. This indicates that the data acquisition is actually set to bipolar, which should be easily fixed.

A method must be developed to calibrate the light sources as well as the source-to-sample separation. If the signals are properly calibrated, a composite redox or hemoglobin ratio image can be created in Matlab™ by first comparing the images, and then creating an algorithm to shift the pixels before averaging.

7. CONCLUSIONS

The redox scanner still requires further work, but the all of the current problems seem solvable, whereas at the beginning of SUNFEST the list of known bugs was overwhelming. The implementation of the DOS computer solved the most critical and demoralizing problem in the system, so it is estimated that future work will be much more easily accomplished. Current test data are very encouraging and may herald the end of the construction phase of the redox scanner. The next phase will involve testing on an animal model to find the efficacy of the sensors on actual biological systems.

8. ACKNOWLEDGMENTS

I would like to thank Dr. Jan Van der Spiegel for his excellent support and chairing of the SUNFEST program, and Ms. Lois Clearfield for her wonderful administration and patience. I extend my sincere appreciation to everyone at the lab for their encouragement and help, especially Lanlan Zhou for introducing me to the redox scanner, Emily Hwang for performing much of the initial work, and Samantha Gaw for her constant assistance, supervision, and dedication to the project. I want to congratulate Dr. Britton Chance, as he is the inspiration for the entire lab and will outlive us all. Finally, I would like to thank the National Science Foundation for supplying the REU grant; without their support this SUNFEST project would not be possible.

9. REFERENCES

1. B. Tromberg, Development of diffuse optical spectroscopy for quantitative characterization of thick tissues, BCMCXC Symposium, Philadelphia, PA, USA, July 2003.

2. B. Chance, E. Anday, S. Nioka, S. Zhou, L. Hong, K. Worden, C. Li, T. Murray, Y. Ovetsky, D. Pidikiti, and R. Thomas, A novel method for fast imaging of brain function, non-invasively, with light, *Op. Ex.*, 2 (1998) 411-423.

3. N. Ramanujam, J. Chen, K. Gossage, R. Richards-Kortum, and B. Chance, Fast and non-invasive fluorescence imaging of biological tissues in vivo using a flying-spot scanner, *IEEE T-BME*, 48 (2001) 1034-1041.

4. B. Chance and H. Baltscheffsky, Binding of intramitochondrial reduced pyridine nucleotide. *J. Biol. Chem*., 233 (1958) 736-739.

5. R. Weissleder, C. Tung, U. Mahmood, Bogdanov, In vitro imaging of tumors with protease-activated near-infrared fluorescent probes*, Nature Biotech*., 17 (1999) 375-378.

6. S. Nioka, *NIH grant proposal for an updated redox scanner*, 2001.

7. B. Chance, H. Schleyer, and B. Schoener, Low temperature excitation and emission spectra of NADH in mitrochondria and tissues, *Biophy. Soc. Abstr.,* TE-8(1963).